Chemical Papers (2021) 75:5421–5433
https://doi.org/10.1007/s11696-021-01731-7

ORIGINAL PAPER

# Composites based on graphite oxide and zirconium phthalocyanines with aromatic amino acids as photoactive materials

Yuriy Gerasymchuk[1] · Leili Tahershamsi[1] · Robert Tomala[1] · Anna Wedzynska[1] · Viktor Chernii[2] · Iryna Tretyakova[2] · Izabela Korona-Glowniak[3] · Barbara Rajtar[4] · Anna Malm[3] · Dominika Piatek[5] · Anna Lukowiak[1]

Received: 20 February 2021 / Accepted: 5 June 2021 / Published online: 14 June 2021


## Abstract

This article is a part of a scientific project focused on obtaining a new type of composite materials that are characterized by singlet oxygen generation upon irradiation with red light, which can be used as antibacterial agents. The composite material is nanoscale graphite oxide (GO) particles covalently bonded to an axially substituted zirconium phthalocyanine complex. For this purpose, two phthalocyanine zirconium complexes, axially mono-substituted with 4-aminosalicylic or 4-aminophthalic acids, were prepared and measured in terms of structure, morphology, and spectroscopic properties. The zirconium phthalocyanines are photosensitizers, and the axial ligands are bridging links connecting the complexes to the GO carrier (due to their terminal amino groups and carboxyl groups, respectively). The axial ligand in zirconium phthalocyanine complexes has a strong influence on the stability and optical properties of composite materials and, consequently, on reactive oxygen species (ROS) generation. In this paper, the effect of composite components (4-aminophthalato or 4-aminosalicylato substituted zirconium phthalocyanine complex as a photosensitizer and graphite oxide as a carrier and modulator of the action of active components) on ROS generation for potential antibacterial use is discussed.

**Keywords** Axially monosubstituted zirconium phthalocyanine · Graphite oxide · Optical properties · ROS generation · Antimicrobial activity · Genotoxicity

## Introduction

The acquired bacterial resistance to antibiotics is one of the biggest problems of medicine (Zaman et al. 2017; Aslam et al. 2018; Nathan 2020; Frieri et al. 2017). Today, scientists are intensively looking for new materials that could effectively replace antibiotics, due to controlled bactericidal, bacteriostatic or antiseptic effect (Cheng et al. 2014; Ghosh et al. 2019). Thus, the photodynamic antibacterial therapy is one of the modern promising methods to kill various microbes or germs (not only bacteria but also fungi and mycoplasma) (Goldman 2007). Very important for photodynamic therapy and diagnostics of microbial infections are photoactive photosensitizers based on macrocyclic compounds, mainly on porphyrins and phthalocyanines (Nyamu et al. 2018; Gao et al. 2018; Mantareva et al. 2013). They are used to treat severely healing wounds, bacterial dermatitis, and mucous membranes (Dougherty 2002; Wainwright 1998; Cieplik et al. 2018), and have recently found application in conservative dentistry and endodontics (Kikuchi et al. 2015; Carrera et al. 2016). Dentists practice shows that in the process of root canal treatment, quite often the secondary infection of the canal takes place. This problem can be caused by inaccurate purification (disinfection) of canals, untight fulfillment of canal or incidence of bacterial strains (especially anaerobic) in the canals, which are resistant to conventional disinfectants and antiseptics therapy (Sundqvist et al. 1998).

✉ Yuriy Gerasymchuk
y.gerasymchuk@intibs.pl

1 Institute of Low Temperature and Structure Research, Polish Academy of Sciences, ul. Okolna 2, 50-422 Wroclaw, Poland

2 V.I. Vernadskii Institute of General and Inorganic Chemistry, 32/34 Palladin Ave., Kyiv 03-142, Ukraine

3 Department of Pharmaceutical Microbiology, Medical University of Lublin, Chodzki 1, 20-093 Lublin, Poland

4 Department of Virology, Medical University of Lublin, Chodzki 1, 20-093 Lublin, Poland

5 Department of Conservative Dentistry and Endodontics, Medical University of Lublin, Al. Raclawickie 1, 20-059 Lublin, Poland

To solve this problem, we have proposed new composite materials based on graphite oxide as a carrier modified with photosensitizer (axially substituted phthalocyanine Zr(IV)) and optionally with nanometric silver (Gerasymchuk et al. 2016). The composition of the material was chosen to strengthen the action of each ingredient:

(1) Graphite oxide—a nanosized carrier and catalyst of silver nanoparticles (Ag-NPs) formation, which shows antibacterial properties and enhances the antimicrobial activity of silver (Gerasymchuk et al. 2017; Lukowiak et al. 2019; Tahershamsi et al. 2020; Kędziora et al. 2013; Saladino et al. 2020);
(2) Ag-NPs—the antibacterial activity of silver is well known, but when the silver is in the form of nanoparticles, this action is more efficient due to an increased contact area further magnified by the GO presence (Kędziora et al. 2013; Kędziora et al. 2020);
(3) Zirconium(IV) phthalocyanine complex (ZrPc) with axial ligands—macrocyclic water soluble metal complex (dye) which plays a role of a photosensitizer and generates singlet oxygen upon light irradiation (Tomachinski et al. 2003; Tomachynski et al. 2004; Gerasymchuk et al. 2021).

Axial ligands in the investigated complexes should contain terminal amino groups that allow covalent linking with the carrier graphite oxide which has various terminal oxygen containing groups. In the previous studies, we have used bis-substituted (i.e. containing two axial ligands coordinated to the central metal atom of metal-phthalocyanine) zirconium phthalocyanine complexes, $L_2ZrPc$, where L = L-lysine, L-arginine, 4-aminobutyric, 11-aminoundecanoic, 3-aminobenzoic, 2,5-diaminobenzoic, nicotinic and isonicotinic acids (Gerasymchuk et al. 2017; Lukowiak et al. 2019; Tahershamsi et al. 2020; Kędziora et al. 2013), which are representing different types of amino acids—aliphatic, aromatic, heterocyclic, and naturally occurring *L*-*α*-amino acids.

In the proposed composites, we embody the idea of stable (not decomposable in tissues) agents, which have a sustained and non-invasive light activated antimicrobial activity. The covalent binding of a phthalocyanine photosensitizer to carrier also reduces its cytotoxicity to eukaryotic cells in tooth and periodontium tissues. One of the aforementioned complexes—bis(lysinato)ZrPc, has been already tested in vitro as a cytostatic agent on cancer cell cultures (Tomachinski et al. 2003). The preliminary results showed that bis(lysinato)ZrPc have blocked growth and/or proliferation of cancer cells which was enhanced by irradiation and can also demonstrate a cytostatic effect against highly resistant pathogenic bacteria. That's why we expected that new ZrPc complexes will have bacterial growth-inhibitory activity and germicidal effect also against pathogenic bacteria obtained from infected root canals, and may find application in dentistry (Tomachynski et al. 2004; Gerasymchuk et al. 2021). As previous studies have shown, the antibacterial effect depends directly on the ability of phthalocyanine complexes (as well as composite material) to generate reactive oxygen species (ROS).

This work is a continuation of the search for bioactive materials based on highly oxidized graphite oxide modified with photosensitizers. As active species, we have chosen complexes of zirconium(IV) phthalocyanine mono-axially substituted with 4-aminophthalic (APhA) or 4-aminosalicylic (ASA) acids (Fig. 1). The goal of the research was to synthesize the material, determine the generation of ROS during light irradiation, and evaluate in vitro the antimicrobial and cytotoxic activities of the studied materials. Genotoxicity tests were also designed to detect if compounds can directly or indirectly cause genetic damage by different mechanisms. Together with our partners involved in the study of the antimicrobial activity of composite materials, we have established that in the first stage we will obtain

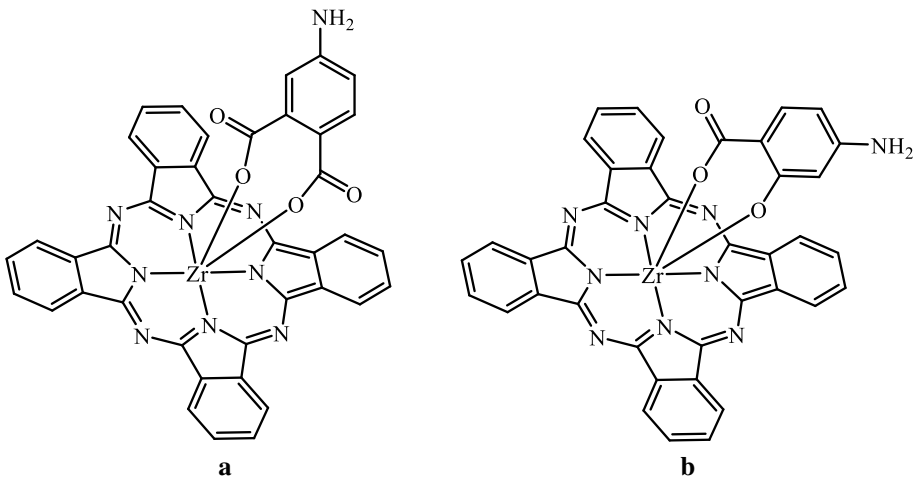


**Fig. 1** Structure of PcZr(4-aminophthalate) (**a**) and PcZr(4-aminosalicylate) (**b**)

composites containing only graphite oxide and a photosensitizer, and if in preliminary tests (MIC, MBC) they show relatively high activity, then this the material will be additionally modified with silver nanoparticles. Due to the fact that the results of the preliminary microbiological esters were not very promising, in this work we did not use and describe additional modification of the examined composite materials with silver nanoparticles.

## Experimental

### Materials and methods

#### Synthesis of materials

All used reagents with ≥ 99% purity were purchased from Alfa-Aesar, USA, and were used without further purification.

Zirconium phthalocyanine complexes axially substituted with one 4-aminophthalic (PcZr(APhA)) or 4-aminosalicylic acid (PcZr(ASA)) ligands, were synthesized by three-stage reaction, according to the reaction scheme shown in Fig. 2. At the first stage, dichloro zirconium phthalocyanine was prepared by the template synthesis method described previously (Tomachynski et al. 2001; Chernii et al. 2003; Gerasymchuk et al. 2004). Then (second step), chlorine atoms were substituted by alkanoate ligands and dialkanoatozirconium phthalocyanine (Tomachynski et al. 2008) was obtained. In the third stage, two alkanoate ligands were substituted by one 4-aminosalicylic or 4-aminophthalic ligand. To achieve the desired complex, 0.33 mmol of $(C_9H_{19}COO)_2ZrPc$ was dissolved in 2 mL of toluene and was added to the suspension of 0.33 mmol of 4-aminophthalic or 4-aminosalicylic acid in 1 mL of toluene. The mixture was boiled under reflux for 1 h. The precipitate was filtered off, washed with toluene and methanol, and finally dried in vacuum at 60 °C (yield about 90%).

Highly oxidized graphite oxide was obtained by oxidation of synthetic graphite with fuming nitric acid and potassium chlorate (Szabó et al. 2006). The carboxyl groups of the obtained GO were activated by standard methods used in the chemical synthesis of peptides in the presence of

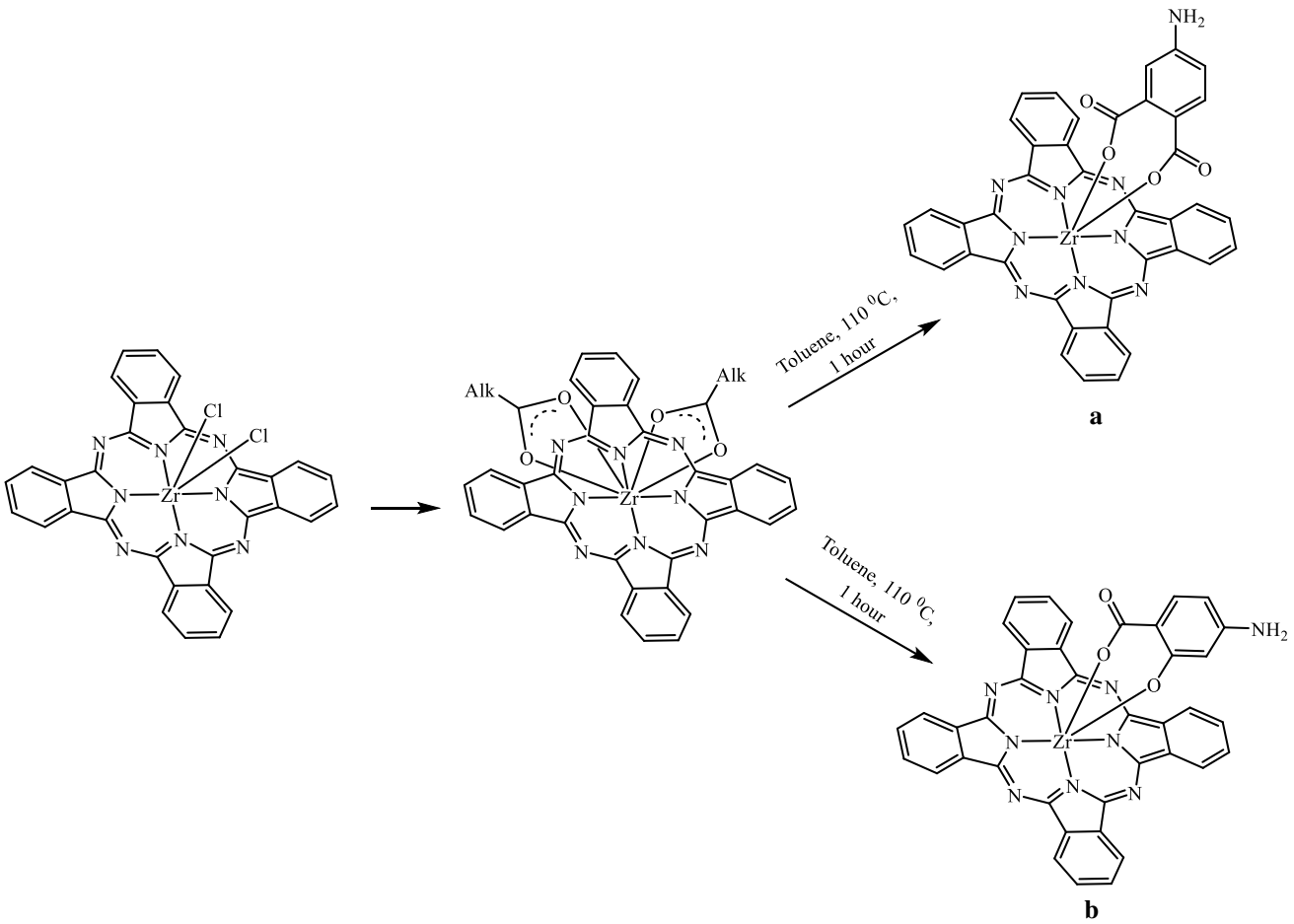


**Fig. 2** Scheme of synthesis of axially mono-substituted zirconium phthalocyanine complexes: PcZr(APhA) (**a**) and PcZr(ASA) (**b**)

dicyclohexylcarbodiimide (DCC) and were reacted with amine group-containing phthalocyanines to form an amide bond (Gershkovich and Kibiriev 1992; Nwahara et al. 2018).

### Physicochemical measurements

The properties of obtained phthalocyanine complexes and composite materials were examined by the following methods:

(1) Elemental analysis of the obtained complexes were carried out by burning method with 2400 CHNS Organic Elemental Analyzer (PerkinElmer) and determination of Zr was realized by ICP-OES method with ICP-OES iCAP 7000 by Thermo Scientific. The following values for the complexes were obtained: Anal. calc. for $C_{40}H_{21}N_9O_4Zr$, PcZr(APhA) (%): C, 61.37; H, 2.70; N, 16.10; Zr, 11.65; found: C 61.29%, H 2.66%, N 15.99%, Zr 11.85%. Anal. calc. for $C_{39}H_{21}N_9O_3Zr$, PcZr(ASA) (%): C, 62.05; H, 2.80; N, 16.70; Zr, 12.08 found: C 61.98%, H 2.78%, N 16.90%, Zr 13.16%.
(2) 1D $^1$H-NMR spectra were recorded with 400 MHz AMX Bruker NMR, and probes were prepared by dissolving of 5 mg of investigated phthalocyanine complex in 0.6 mL of DMSO-$D_6$ in NMR Scientific tubes (Roth, Germany). Tetramethylsilane was used as an internal standard.
(3) X-ray diffractograms were recorded from material powders by powder diffractometry with X'Pert Pro diffractometer by PANalytical.
(4) Scanning electron microscopy images were obtained from probes deposited from methanol suspension on graphite plates with FESEM (FEI Nova NanoSEM 230).
(5) FT–IR spectra were recorded with FT–IR spectrometer Biorad 575C. Probes were prepared by grinding of investigated material with KBr and forming into pellet.
(6) UV–Vis-NIR absorption spectra were recorded in 1 cm quartz cuvettes with Agilent CARY 5000 UV–Vis-NIR spectrometer for solution/suspension of investigated materials in saline (Braun, Germany) and spectroscopy grade DMSO (Alfa-Aesar, USA). Solution (in case of free phthalocyanine complex) or suspension (in case of GO samples) in spectroscopy grade DMSO was prepared with UZDN M900-T (900 W, 22 kHz) disperser. Absorption spectroscopy was also used for the analysis of the reactive oxygen species generation of free phthalocyanine solutions and composite suspensions in DMSO in the presence of 1,3-diphenylisobenzofuran (DPBF) under red/NIR light irradiation. Philips 150 W lamp with wavelength range between 550 and 900 nm with the maximum at around 700 nm was used as red/NIR irradiation light source. The samples were irradiated with a wide-band red lamp in short intervals (from 10 to 240 s) from a distance of 50 cm according to the method described in (Avşar et al. 2016). For the convenience of results comparison, selected spectra were normalized.
(7) Photoluminescence spectroscopy measurements were carried out with Spectrophotometer FLS980 Edinburgh Instruments (supported with xenon lamp and appropriate optical filters) in 1 cm quartz cuvettes; molar concentration of free phthalocyanine complexes solution in DMSO was $C_m = 5 \cdot 10^{-6}$ M, whereas concentration of composite in DMSO suspension was $C = 0.1$ g/L.

### Antimicrobial activity assay in vitro

The complexes were screened for antibacterial and antifungal activities by micro-dilution broth method using Mueller–Hinton broth for growth of bacteria or Mueller–Hinton broth with 2% glucose for growth of fungi (Gacki et al. 2020). Minimal inhibitory concentration (MIC) of the tested derivatives was evaluated for the panel of the reference microorganisms from American Type Culture Collection (ATCC), including Gram-negative bacteria (*Escherichia coli* ATCC 25,922, *Salmonella* Typhimurium ATCC14028, *Klebsiella pneumoniae* ATCC 13,883, *Pseudomonas aeruginosa* ATCC 9027, *Proteus mirabilis* ATCC 12,453), Gram-positive bacteria (*Staphylococcus aureus* ATCC 25,923, *Staphylococcus aureus* ATCC 6538, *Staphylococcus epidermidis* ATCC 12,228, *Micrococcus luteus* ATCC 10,240, *Bacillus subtilis* ATCC 6633, *Bacillus cereus* ATCC 10,876) and fungi (*Candida albicans* ATCC 10,231, *Candida parapsilosis* ATCC 22,019, *C. glabrata* ATCC 90,030). The complexes dissolved in deionized (DI) water were first diluted to the concentration (100 mg/mL) in an appropriate broth medium recommended for bacteria or yeasts. The microplates (with bacteria and tested samples) were irradiated for 5 min (with the same irradiation source as for ROS generation measurements). Before irradiation the bacteria with tested samples were incubated at room temperature within 10 min. For comparison, vancomycin, ciprofloxacin, and nystatin were tested as the standard drugs against Gram-positive, Gram-negative bacteria, and yeasts, respectively (Table S1).

### Cytotoxicity assay

The Vero cell culture (ATCC No. CCL-81) established from the kidney of a normal adult African Green monkey was used in the experiment. The cell medium (Dulbecco's Modified Eagle Medium—DMEM (Corning), supplemented with 10% foetal bovine serum (FBS, Capricorn), 100 µg/mL penicillin and 100 µg/mL streptomycin solution (Corning) was used for culturing cells.

The tested samples were diluted in $H_2O$ until the final concentration of 50 mg/mL. The cell culture was seeded into 96-well plastic plates (NUNC, Denmark). The plates were filled with 100 µl suspension of Vero cells at a density of $1.5 \times 10^4$ cells per wall, prepared on the culture medium with 10% serum. After 24 h incubation at 37 °C, the medium was removed from the culture and the tested samples, diluted in a culture medium with 2% serum, were added. Twofold serial dilutions of compounds, from 2 to 0.001 mg/mL, were added to the cells in triplicates. The culture medium with 2% serum only was added to the cell medium control. The samples were diluted at a limited exposure to light. The cells subject to substance were exposed to NIR light 5 times for 1.5 min with 1-min intervals and then incubated for 24 h at 37 °C in the 5% $CO_2$ atmosphere.

The substance cytotoxicity was evaluated with the MTT formazan test (Rajtar et al. 2017). On the basis of cell measurement, the $IC_{50}$ of the testing substance—the concentration which caused 50% reduction of the cell activity compared to the control, was determined.

#### Genotoxicity test

1-Day Microplate Format Genotoxicity Assay (umuC Easy CS, Xenometrix, Swiss Commitment for Bioassays) for testing of concentrated substances using *S. typhimurium* TA1535/pSK1002 with media and reagents as described in ISO 13,829 was used according to manufacturer's instruction. *S. typhimurium* TA1535 [pSK1002] bacteria in the exponential growth phase were exposed for 120 min to 4 concentrations of a test sample: 4, 2, 1, 0.5 mg, as well as to a positive and a negative control. After 2 h, the exposure cultures were diluted in fresh medium and allowed to grow for another 2 h. The induction and expression of the umuC—lacZ reporter gene were then assessed after lysis of the bacteria. Colorless ortho-nitrophenyl-$\beta$-galactoside (ONPG) is converted to the yellow o-nitrophenol product in the presence of induced $\beta$-galactosidase (lacZ). The intensity of the color correlates with the amount of $\beta$-galactosidase present and thus with the genotoxic potency of the tested compound. Measurement of the OD600 before and after the 2 h growth phase allowed to calculate an induction ratio and to identify toxic growth inhibitory effects. The genotoxic potential of substances was assessed directly or in the presence of liver S9 fractions.

## Results and discussion

### Synthetic part

In comparison with the synthesis of zirconium phthalocyanine complexes described in our earlier works (Tomachynski et al. 2001; Chernii et al. 2003), where the yield reached 60–80%, phthalocyanine complexes with phthalic acid and 5-sulfosalicylic, both complexes (PcZr(APhA) and PcZr(ASA)) containing amino groups in the axial substituent were formed under similar conditions with higher yields of about 90%. The formation of complexes of amino acids with PcZr also plays the role of a protective reaction of the carbonyl group. Since the obtained complexes are highly stable, this gives us the opportunity to use DCC to activate the graphite surface and then to form an amide bond with the amino group in the complex.

### NMR spectra

In the NMR spectra of both complexes, there are two signal groups (Figs. S1 and S2 in Supplementary Information). First of them consists of two multiplets at 9.50–9.33 and 8.32–8.17 ppm and can correspond to $H^a$ and $H^b$ protons of Pc-cycle, respectively. The second group of signals corresponds to out-off-plane ligands. Signals of aromatic protons were in the range of 7.80–5.90 ppm. For PcZr(APhA), there are observed the following signals: the singlet at 7.83, the multiplet at 6.80–6.55, and the multiplet at 6.05–5.80 ppm that can correspond to H6, H5, and H3 protons of 4-aminophthalic fragment, respectively. The singlet signal at 5.20 ppm corresponds to amino group protons. The total ratio of signal integral intensity for PcZr(APhA) is 8:8:1:1:1:2. For PcZr(ASA) the situation is similar with three signals: the doublet at 7.42, the doublet at 6.42, and the multiplet at 6.10–5.92 ppm that can correspond to H6, H5, and H3 protons of 4-aminosalicylic fragment, and amino group, respectively. The total ratio of integral intensity for PcZr(APhA) is 8:8:1:1:3. The proton signals of the starting compounds (reagents) were not identified in the spectra.

### Mass spectroscopy (ESI–MS)

In the mass spectra of both complexes, there are intense molecular ion signals present at m/z equal to 754.09 and 787.56 for PcZr(ASA) and PcZr(APhA), respectively (Figs. S3 and S4 in Supplementary Information). Other identified signals are at m/z = 899.26 for PcZr(ASA) and m/z = 928.74 for PcZr(APhA)—their presence indicates that two solvent molecules (DMF) enter the coordinating sphere of zirconium, which confirms our earlier research on complexes of axially substituted zirconium phthalocyanines (Tahershamsi et al. 2020; Tretyakova 2007). Fragmentation of the complex takes place in the following mode: in the first stage, the axial ligand is disconnected and a $PcZrO_2$ complex is formed with m/z = 637.78, followed by demetallation of the complex confirmed by the presence of the signal of free phthalocyanine at m/z = 515.82.

## X-ray diffractometry and SEM images

X-ray diffractometry and scanning electron microscopy were used for the evaluation of the structure and morphology of the graphite oxide carrier and composites. The GO flakes have widths of 0.5–5 µm which have not been changed after deposition of complexes (Fig. 3).

The strong diffraction line at $2\Theta = 11.6°$ (Fig. 4) corresponds to an interlayer spacing of about 0.76 nm, indicating the presence of oxygen functional groups, which facilitated the oxidation and exfoliation of graphene sheet in aqueous media. Slight changes in the material structure are visible in the X-ray diffraction patterns, which indicates a partial reduction of graphite oxide during the functionalization reaction conditions. The reaction of deposition of phthalocyanine complexes on the carrier is coupled with a slight reduction of graphite oxide, and the hydrophilicity of water-dispersed GO sheet gradually decreased, leading to an irreversible agglomeration of partially reduced graphene oxide sheet. The weak and broad reflection at $2\Theta = 25.8°$ indicates a random clumping of graphene sheets in the partially reduced graphite oxide. This line is corresponding to the 002 plane of graphite with interlayer spacing of 0.34 nm which is due to the removal of oxygen atoms that got into the graphite gallery during the intercalation process (Thema et al. 2013). On the one hand, the appearance of this signal confirms the reduction process of graphite oxide, but on the other, the very low intensity of the line at $2\Theta = 25.8°$ indicates that graphite oxide is reduced to a very low degree during the deposition reaction of zirconium phthalocyanine complexes. X-ray diffraction studies as well as microscopic imaging of the samples indicate that the composite materials GO-Pc(ASA) and GO-Pc(APhA) do not differ structurally and morphologically.

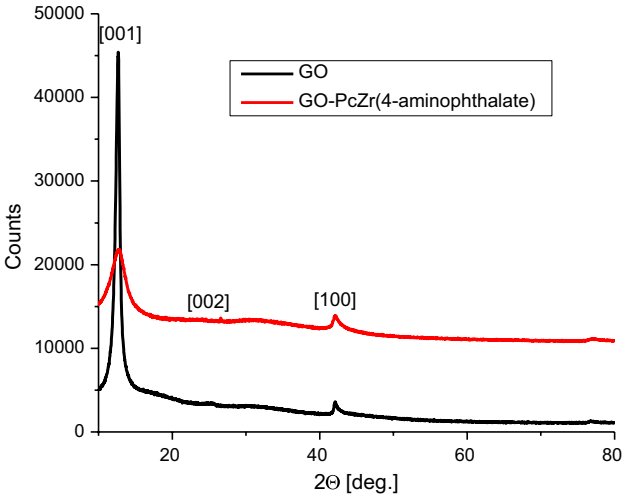


**Fig. 4** XRD diffractograms of graphite oxide (black line) and GO-PcZr(4-aminophthalate) composite (red line)

## FT–IR spectroscopy

The FT–IR spectra were recorded to confirm ligand exchange in the phthalocyanine complexes (Figs. S5 and S6 in Supplementary Information) (Chernii et al. 2003; Gerasymchuk et al. 2004; Tomachynski et al. 2008).

The Zr–O bands in the FT–IR spectra are shown at $\upsilon_{as} = 783\ cm^{-1}$ and $\upsilon_{s} = 777\ cm^{-1}$. Also the bonding of phthalocyanine complexes to GO is confirmed by a characteristic mode at 1300–1230 $cm^{-1}$ region related to the CO–NH

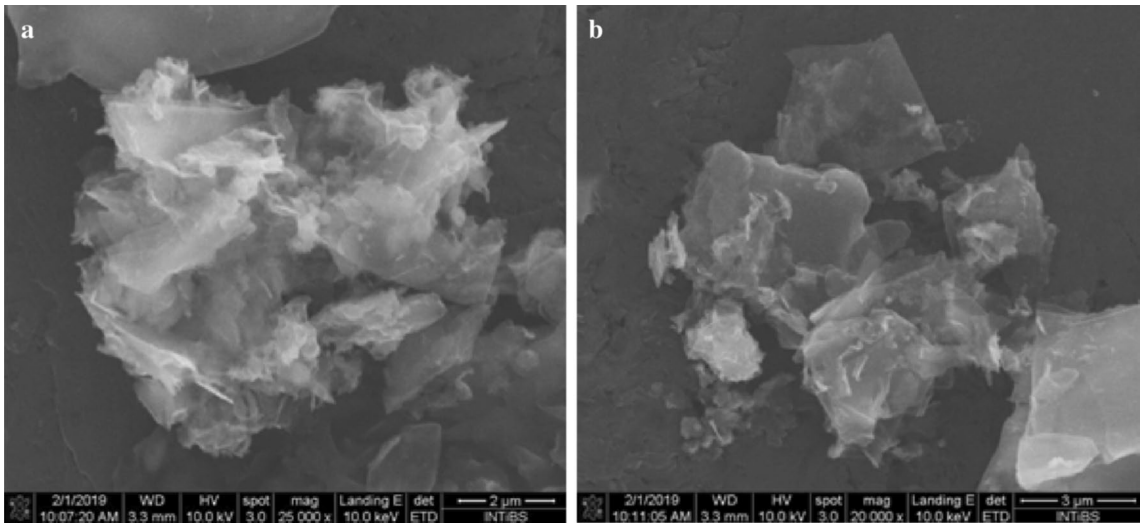


**Fig. 3** SEM images of graphite oxide (**a**) and composite material (GO-PcZr(4-aminophthalate)) (**b**)

amide bond. Slight deviations in the position of characteristic bands (Table 1) derived from ligands in the free complex and from the same complex but in composite material result from the covalent bonding with GO carrier. Simultaneously, much lower intensity of these bands reflects low content of the phthalocyanine complex in the composite.

## UV–VIS-NIR absorbance measurements

Absorption spectroscopy was used for the additional confirmation of the presence of the photosensitizer in the composite. The Q bands of phthalocyanines with $\lambda_{max}$ at 685 nm are seen in the spectra of both composites' suspensions in DMSO (Fig. 5). The bands are slightly shifted (from 685 to 689 nm) in comparison with the free Pcs solutions. Satellite band of phthalocyanine in composite material also shows hyperchromic shift (from 617 for free complex to 623 nm for composite). High absorbance seen in the case of composites

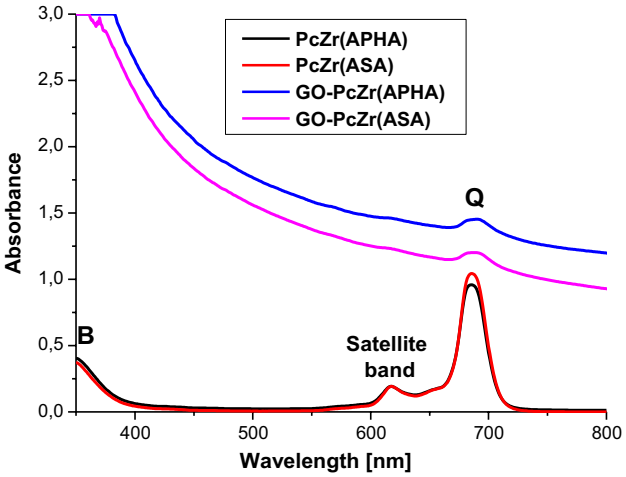


**Fig. 5** Absorption spectra of PcZr complexes and corresponding GO composites in DMSO

**Table 1** Main FTIR signals of phthalocyanine complexes and composite materials

| PcZr (4-aminophthalate) | GO-PcZr (4-aminophthalate) | PcZr (4-aminosalicylate) | GO-PcZr (4-aminosalicylate) | Types of vibrations |
|---|---|---|---|---|
| 3327 m, 3188vw | 3433vw, 3381w | 3326 m, 3185vw | 3458b, 3385 m | $\nu$(C-N) |
| 3127vw, 3061vw, 3034vw | 3231vw, 3084vw, 3061vw | 3124vw, 3034vw | 3334vw, 3227vw, 3082vw, 3061vw, 3052vw | $\nu$(CH)-aromatic |
| 2945sh, 2928w, 2916sh, 2852vs | 2950sh, 2928w, 2849w, 1729 m, 1717 m | 2946vw, 2930vw, 2850vw | 2946sh, 2929vw, 2850vs, 1722b | $\nu$(COO) |
| 1654sh, 1626 m, 1575vs, 1536 m | 1621sh, 1604 s, 1524w | 1632 s, 1609 m, 1577 m | 1633 s, 1609 m, 1578 m | $\nu(CO)+\nu(\varphi)+\delta(NH_2)$ |
| 1497 m, 1477w, 1460sh | 1502 s, 1478vw, 1466vw | 1499vs, 1456 s | 1499vs, 1456 s | $\nu(CNC)+\nu(\varphi)+\delta(CH)$ |
| 1449sh, 1436 m, 1417 m, 1386w, 1346 s | 1419w, 1340vw, 1381sh | 1416w, 1384w, 1333vs | 1416w, 1384w, 1332vs | $\nu(\varphi)+\delta(CH)$ |
| 1311 s | 1332vs, 1289vs | 1300sh, 1289vs | 1300sh, 1289vs | $\nu(CNC)+\delta(ZrN_4)+\nu(\varphi)+\nu(CN)$ |
| 1271 m, 1244 s, 1230 m | | 1248vw, 1227w | 1248vw, 1227w | $\delta(CO)+\nu(\varphi)+\nu(CNC)+\delta(CH)$ |
| 1186w, 1158w, 1118sh | 1190vw, 1163vs, 1119 s | 1197w, 1164vs, 1119vs | 1197w, 1164vs, 1119vs | $\delta(CH)+\delta(ZrN_4)+\nu(\varphi)$ |
| 1088 s, 1068 s, 1045 s | | 1074 s | 1074 s | $\delta(CH)+\delta(\varphi)+\rho(ZrN_4)$ |
| | 1075 s | 1074 s | 1074 s | GO |
| 967vw, 957sh, 955vw, 946sh | 1006ww, 986ww, 955vw | 1001vw, 976w, 966sh | 1002vw, 976vw, 965vw | $\delta(CH)+\delta(\varphi)+\rho(ZrN_4)$ |
| 903w, 892 s, 843vw | 892vs, 867vw, 842vw, 825 s | 893 s, 878vw, 868vw, 854vw | 894 s, 878vw, 862sh, 857vw | $\gamma(CH)+\delta(\varphi)+\delta(CNC)+\delta(CN)$ |
| 802 m | 793sh, 780 m | 827 m, 789Sh, 779w, 748vs | 791sh, 779 s | $\gamma(CH)+\delta(ZrN_4)+\gamma(\varphi)$ |
| 780 s | 780 s | 783vw | 779 s | $\nu_{as}$(Zr–O) |
| 774vw | 774vw | 777vw | | $\nu_{s}$(Zr–O) |
| 725vw | 748vs, 736vs | 735vs, 726sh, 702w | 748vs, 735vs, 726sh, 702 m | $\delta(\varphi)+\delta(CNC)+\gamma(\varphi)$ |
| 653w, 640 s | 668sh, 650vw, 642vw | 667sh, 638w | 668sh, 638w | $\gamma(\varphi)+\gamma(CH)+\delta(CNC)+\rho(ZrN_4)$ |
| 537w | 537vw, 506 m | 584w, 567w, 536w | 584w, 567w, 535w | $\delta(\varphi)+\gamma(CH)+\delta(CNC)+\rho(ZrN_4)$ |
| 447w | 417vw | 421vw | 437w, 431 s | $\delta(CNC)+\rho(ZrN_4)+\gamma(\varphi)+\gamma(CH)$ |

Key: vs—very strong; s—strong; m—medium; w—weak; vw—very weak; b—broad; sh—shoulder; $\varphi$, ring; $\nu$, stretching vibration; $\rho$, rocking vibration; $\delta$, deformational or in-plane bending vibration; $\gamma$, out-of-plane vibration

and increasing with shorter wavelength is caused by the GO flakes present in the solvent.

Due to the fact that these materials are considered to be used in systems where the basic medium is water (physiological fluids), we conducted the Lambert–Beer experiment to determine the dependence of absorption intensity on Pcs concentration. The experiment was carried out for the studied phthalocyanine complexes in saline. For a comparison, an analogous measurement was carried out in a DMSO solution.

A strong dimerization (aggregation) of the complex takes place in aqueous solutions as a result of the constriction of $\pi$-systems of phthalocyanine rings that is observed as change in the shape of the spectrum in the Q band: peak shifts (the maximum of the satellite band from 617 to 640 nm, and the main Q band from 687 to 697 nm) and the increase in absorption intensity for the satellite band and a decrease for the main Q band (Figs. 6, 7, 8, 9) (Gerasymchuk et al. 2004; Tretyakova et al. 2007). As has been shown in our earlier work, the use of saline instead of distilled water reduces aggregation of axially substituted zirconium phthalocyanine complexes (Gerasymchuk et al. 2021) and also makes it possible to evaluate photoactivity under conditions similar to biological conditions. In the case of the PcZr(APhA) complex, agglomeration processes were observed not only for the water environment, but also in a DMSO solution (Fig. 8)—the linear regression coefficient $R^2$ was 0.9318, which proves a greater deviation from the Beer–Lambert law than in the case of PcZr (ASA), for which the linear regression coefficient $R^2$ was 0.9968, i.e. practically close to 1. Admittedly, agglomeration is observed at quite high

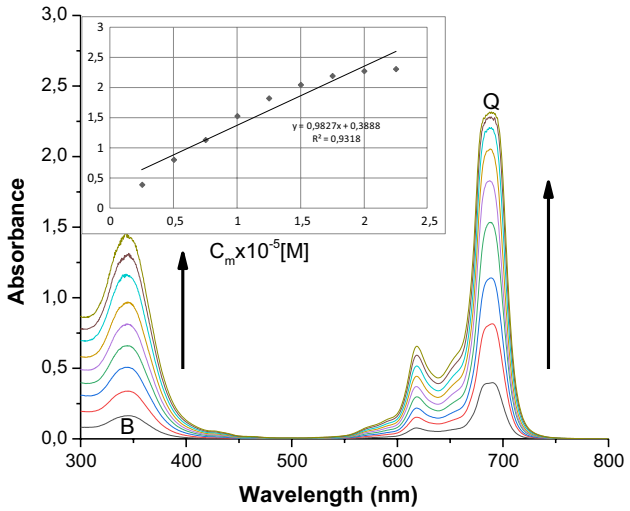


**Fig. 6** Lambert–Beer linearity experiment for PcZr(APhA) in DMSO. Inserted graph shows the dependence of the intensity of the Q-band maximum absorption at 688 nm on the concentration of PcZr(APhA) and the specified coefficients of the Lambert–Beer law linearization

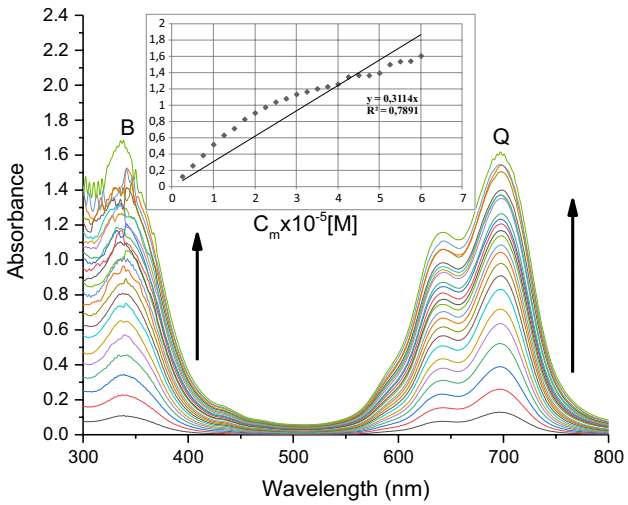


**Fig. 7** Lambert–Beer linearity experiment for PcZr(APhA) in saline. Inserted graph shows the dependence of the intensity of the Q-band maximum absorption at 697 nm on the concentration of PcZr(APhA) and the specified coefficients of the Lambert–Beer law linearization

concentrations (above $10^{-4}$ M), but it does occur. It is interesting that for PcZr(ASA), and for none of the previously studied complexes (Tahershamsi et al. 2020; Gerasymchuk et al. 2004; Tomachynski et al. 2008; Tretyakova et al. 2007), agglomeration in DMSO was not observed in a much wider range of concentrations. It is associated, in our opinion, with the nature of the axial ligand, which, in contrast to those previously studied, has more hydrophobic character.

In aqueous solutions (polar solvents), the complex with 4-aminosalicylic ligand begins to aggregate at much higher concentrations ($> 4 \times 10^{-5}$ M) than PcZr(APhA)

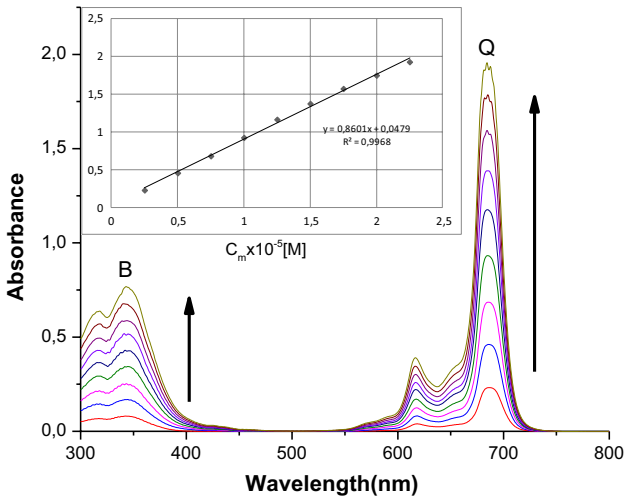


**Fig. 8** Lambert–Beer linearity experiment for PcZr(ASA) in DMSO. Inserted graph shows the dependence of the intensity of the Q-band maximum absorption at 685 nm on the concentration of PcZr(ASA) and the specified coefficients of the Lambert–Beer law linearization

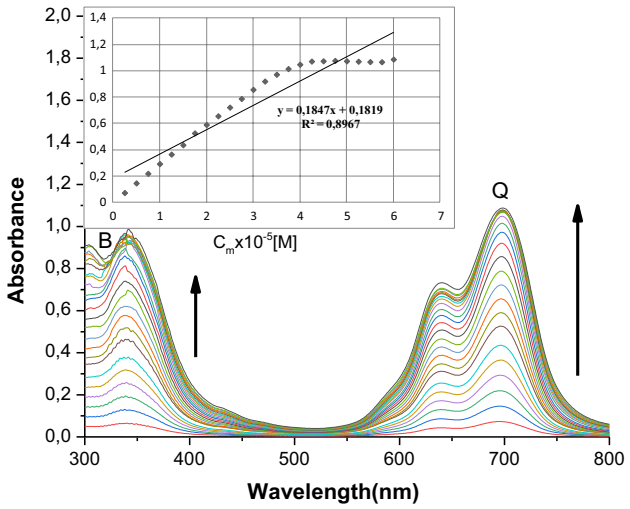


**Fig. 9** Lambert–Beer linearity experiment for PcZr(ASA) in saline. Inserted graph shows the dependence of the intensity of the Q-band maximum absorption at 697 nm on the concentration of PcZr(ASA)

($< 2 \times 10^{-5}$ M) or other axially substituted complexes which we have studied so far (Gerasymchuk et al. 2004; Tomachynski et al. 2008). This is a key result since the aggregation of phthalocyanines in aqueous solutions has a strong negative effect on their spectroscopic properties reducing the efficiency of their luminescence through the concentration effect of self-quenching (Gerasymchuk et al. 2004; Gerasymchuk 2010). The deviation from the linearity of the Lambert–Beer law in the case of aqueous solutions of the studied phthalocyanine complexes is quite large, the coefficients of linear regression fitting $R^2$ were 0.789 for PcZr (APhA) and 0.897 for PcZr (ASA), respectively. We also tried to do a fitting the observed absorbance changes as a function of the complex concentration in order to calculate dimerization constants. However, the obtained results were completely unsatisfactory, which is related to the fact that, monomer–dimer model used for fitting, the model is too simple to describe the processes involved. In fact, the degree of aggregation of the complexes increases as their concentration in solution increases and larger agglomerates form. As a consequence, it also affects the efficiency of ROS generation that is higher for the PcZr(ASA) than for PcZr(APhA).

Dimerization constants were calculated according to (Brozek-Pluska et al. 2016) and are presented in Table 2.

The dimerization constants were significantly higher for the studied complexes in the aqueous environment than in DMSO. The value of this constant for PcZr(ASA) in saline is comparable to the constant for PcZr(APhA) in DMSO solution, which is explained by the fact that we observe aggregation processes for the latter complex in the studied concentration range (both in saline and DMSO).

**Table 2** Dimerization constants calculated for investigated complexes in water medium and DMSO

| Type of ligand in PcZrL complex | Solvent | $K_d$ [L/mol] |
|---|---|---|
| APhA | Saline | $2.12 \times 10^5$ |
| | DMSO | $1.35 \times 10^5$ |
| ASA | Saline | $1.02 \times 10^5$ |
| | DMSO | $0.41 \times 10^4$ |

## ROS generation measurements

For the analysis of the reactive oxygen species generation by the samples, spectroscopy was also used to monitor the intensity of 1,3-diphenylisobenzofuran (DPBF) absorption band changing with the irradiation of the investigated system. The spectra registered after various time of irradiation are presented in Figs. S7 and S8 in Supplementary Information for phthalocyanine complexes dissolved in DMSO, and, respectively, in Figs. S9 and S10 for DMSO suspensions of appropriate composites. Fig. S7 shows the decrease of DPBF absorbance (monitored at 420 nm) during irradiation.

The analysis of the decay of DPBF absorbance depending on the exposure time of the samples indicates that both complexes generate ROS. This activity is slightly lower than for the standard zinc phthalocyanine complex (black pattern in Fig. 10) (Nwahara et al. 2018; Avşar et al. 2016). The PcZr(ASA) generates ROS more intensively than PcZr(APhA). For appropriate composites, this relationship is maintained, although the activity is lower due to much lower PcZr content in the system. We should also notice that no changes in DPBF absorption were observed during

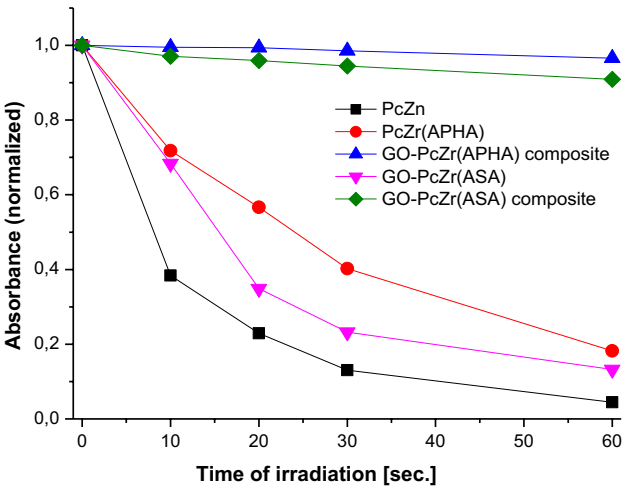


**Fig. 10** Comparison of ROS generation (decrease of DPBF absorbance at 420 nm during light irradiation) by investigated complexes, composites, and PcZn (standard) in DMSO solution

irradiation of GO suspension demonstrating that only PcZr showed this kind of photoactivity.

## Photoluminescent properties

The photoluminescence of all investigated samples clearly demonstrates optical activity of both complexes and composites. In the excitation spectra (Fig. 11), equal for all samples, B and Q bands of Pcs are visible in the UV and red spectrum ranges, respectively (spectra registered monitoring emission at 700 nm). Thus, light from these two spectral ranges might be used for systems' activation. The photoluminescence was measured upon excitation at 620 nm (satellite band). The characteristic emission of Pcs was observed in the range of 650–800 nm (Fig. 11). The emission intensity was significantly lower in the case of composites; nevertheless, it was easily registered, although the PcZr concentration was quite low. The emission intensity of photosensitizers strongly corresponds to the ROS generation and, as a result, to their biological activity (Gerasymchuk et al. 2021; Nyokong and Antunes 2013). Therefore, due to the observed photoluminescence, the photoactivity and ROS generation under red/NIR light exposition was expected and demonstrated for all the samples.

We would like to also present other results which are very interesting, although they are not strictly related to the target use of these materials. These are spectra obtained by excitation of phthalocyanine complexes solutions in DMSO ($C_m = 0.5 \times 10^{-5}$ M) at 345 nm (phthalocyanine Soret band maximum) and registering photoluminescence spectra in the near infrared region (Fig. S11 in Supplementary Information). It turned out that PcZr(APhA) in this range has a different band shape than PcZr(ASA). For PcZr(ASA), the band has a shape rather typical for phthalocyanines when excited into the Soret band, where the signal at 705 nm is more intense, and the less intense component with a maximum at 766 nm, which is a derivative of the satellite band in the Q range. On the other hand, for PcZr(APhA), the ratio of the emission spectrum components is the opposite, and the signal at 771 nm is larger, and the signal at 704 nm is less intense. Such ratio of the bands intensity, as well as the shift of the satellite band to a longer wavelength in excitation spectrum of PcZr(APhA) in comparison with PcZr(ASA) (from 620 to 640 nm), indicates that in a DMSO solution, even at such a low concentration, PcZr(APhA) is highly agglomerated (as it was mentioned above, there exists not only a dimerization process of "face-to-face" type, but rather more advanced agglomeration processes) (Gerasymchuk et al. 2010). By the way, for composite materials, with the same parameters of the excitation wavelength (for emission spectra) and detection (for the excitation spectra) (Figs. S12 and S13 in Supplementary Information), such changes in the phthalocyanine bands were not noticed, which on the one hand could be explained by lower phthalocyanine concentrations, but more likely is the justification that was the starting point for the assumptions for this work, i.e. that the complexes of phthalocyanines covalently bonded to the graphite oxide carrier have no possibility of dimerization or further agglomeration; thus, despite their low content in the systems, the emission efficiency for them will be higher, compared to the unbound forms. It should also be noted that the conducted research did not show a significant increase in emission efficiency due to the antenna effects and charge transfer from graphite oxide. The Stokes shift for phthalocyanine complex solutions was 20 nm for PcZr(APhA) and 18 nm for PcZr(ASA), while for composite materials it was smaller and was 16 nm for GO-PcZr(APhA) and only 5 nm for GO-PcZr(ASA), but the emission intensity for ASA is twice as high. This is due, in our opinion, to the fact that the measuring ranges we are interested in in connection with the theoretical application of these materials are at much higher wavelengths than the graphite oxide excitation maxima, which are close to the measurement limits, i.e. about 190–200 nm.

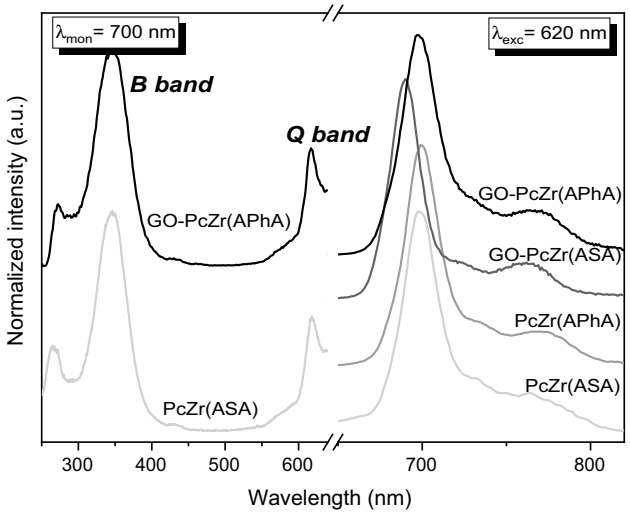


**Fig. 11** Excitation (left) and emission (right) spectra of PcZr complexes (PcZr(ASA) and PcZr(APhA)) and GO-PcZr composites in DMSO

## Cytotoxicity and antimicrobial activity

The cytotoxicity of GO-PcZr(ASA) and GO-PcZr(APhA) on Vero cells was evaluated by MTT assay. The concentrations of complexes inducing 50% reduction in cell viability (mean $IC_{50} \pm SD$) were $0.221 \pm 0.075$ and $0.121 \pm 0.005$ mg/mL, respectively. The composites displayed high antiproliferative activity (IC50 < 1 mg/mL) against Vero cells.

Antimicrobial activity testing against reference strains showed MIC values > 10 mg/mL of tested composites

indicating no bioactivity (Tab. S1 in Supplementary Information). Irradiation showed increase of the composites activity against Gram-positive micrococci and yeasts for GO-PcZr(ASA) and additionally for spore-forming *B. subtilis* for GO-PcZr(APhA) (MIC 5–10 mg/mL).

At first glance, it might seem that the values of concentrations ensuring antimicrobial and antifungal activity of the tested materials are incomparably higher than for the substances (antibiotics and fungicides) used as references (Tab. S1). However, for GO-PcZr(ASA) or GO-PcZr(APhA) composites, the active (or rather photoactive) substance content in the material is estimated to be at the level of – 1%. Therefore, when comparing the results obtained using the same test methods, the actual amount of photoactive substance should be indicated, which would in fact be two orders of magnitude lower in the case of Pcs. In such an assessment of the situation, it might be concluded that the proposed materials have good antimicrobial properties, which can be particularly interesting in the case of their antifungal activity. It is also very important to note that, when using antibacterial photodynamic therapy, different mechanisms of influence on bacteria are activated than in the case of antibiotic therapy. Moreover, PDT is less capable to cause new resistance mechanisms of bacteria. Therefore, research is being actively conducted in such direction to replace, at least to some extent, antibiotic therapy. Besides, these two treatments can be used in parallel, increasing the effectiveness of the entire treatment protocol.

Many factors contribute to the overall antimicrobial activity of GO nanomaterials. It is highly dependent on the materials' properties, including lateral size, purity, structural defects, charge, functional groups, degree of oxidation, and hydrophilicity (Liu et al. 2011). The reason for weak antimicrobial activity of GO-PcZr(ASA) and GO-PcZr(APhA) composites presented in this study may result from their strong aggregation in aqueous solutions. For instance, surfactant dispersed individual single-walled carbon nanotubes (SWCNTs) show higher toxicity to various bacterial cells than nanotube aggregates (Liu et al. 2009). We consider that it could be also applicable to other graphene-based materials. Moreover, Arias and Yang (Arias and Yang 2009) previously reported that the buffer and concentration of SWCNTs are the two key factors that affect their antimicrobial activity. SWCNTs exhibited extremely strong antimicrobial activity only in water or 0.9% NaCl solution but not in phosphate buffered saline and Brain Heart Infusion broth (here, we determined no antimicrobial activity of the composites testing them according to the standard method recommended by EUCAST using Mueller-Hinton broth). Additionally, Liu et al. (2011) suggested that the antibacterial activities of graphene-based materials are attributed to their dispersibility, size, and oxidization capacity. The results presented in this study indicate that both tested complexes generate ROS, but unfortunately the intensity of their generation is lower than for the standard zinc phthalocyanine complex that may have an impact on their antimicrobial activity.

GO-PcZr(ASA) and GO-PcZr(APhA) have also been tested for mutagenicity in Ames study with TA1535. Results from the plate incorporation treatment, up to 4 mg/plate, showed no increase in the frequency of revertant colonies, with all values falling within the expected background range for the strain. Positive controls gave expected results, and as such the test was considered valid. Then, these substances cannot be judged to be mutagens.

## Conclusions

The correctness of the proposed strategy for the synthesis of mono-substituted zirconium phthalocyanine with 4-aminophthalic or 4-aminosalicylic acid as an axial substituent has been proven. Basic structural, morphological, and optical parameters of these complexes as well as their composite material with graphite oxide were characterized.

The PcZr(4-aminosalicylate) complex in aqueous solution begins to aggregate at much higher concentrations than all the axially substituted complexes we have studied so far. This is a key result, since the aggregation of phthalocyanines in aqueous solutions has a strong negative effect on their spectroscopic properties, reducing among others the efficiency of their luminescence through the concentration effect of self-quenching. As a consequence, it also affects the efficiency of ROS generation. By the DPBF bleaching method, it was proved that the PcZr(ASA) complex and its GO-based composite had higher photoactivity than the PcZr(4-aminophthalate) derivatives. Nevertheless, the concentration of ROS generated under the tested conditions was not high enough to ensure antimicrobial effect of the composites. The lack of activity may be also caused by aggregation of GO flakes in the Mueller-Hinton broth. Despite the lack of antibacterial effect, other medical applications of the composites cannot be excluded (e.g. as components of dressing materials or active implant layers).

Our previous experience showed that mono-substituted PcZr complexes usually have higher solubility in polar solvents (due to the geometry of the molecules), as well as higher absorption coefficients and emission intensity, which in our opinion could translate into higher ROS generation capacity and more effective antimicrobial effect. However, these assumptions were proved partially, because despite the intensive generation of ROS under experimental conditions, the impact of composite materials on bacteria turned out to be relatively low compared to the previously studied composites. But on the other hand, these materials were also characterized by low cytotoxicity to eukaryotic cells, which is an essential factor for their further use in medical practice.

**Supplementary Information** The online version contains supplementary material available at https://doi.org/10.1007/s11696-021-01731-7.

**Acknowledgements** This research was funded by the National Science Centre research Grant No. 2016/23/B/ST5/02480.



## References

Arias LR, Yang L (2009) Inactivation of bacterial pathogens by carbon nanotubes in suspensions. Langmuir 25(5):3003–3012. https://doi.org/10.1021/la802769m

Aslam B, Wang W, Arshad MI, Khurshid M, Muzammil S, Rasool MH, Nisar MA, Alvi RF, Aslam MA, Qamar MU, Salamat M, Baloch Z (2018) Antibiotic resistance: a rundown of a global crisis. Infect Drug Resist 11:1645–1658. https://doi.org/10.2147/IDR.S173867

Avşar G, Sari FA, Yuzer AC, Soylu HM, Er O, Ince M, Lambrecht FY (2016) Intracellular uptake and fluorescence imaging potential in tumor cell of zinc phthalocyanine. Int J Pharm 505(1–2):369–375. https://doi.org/10.1016/j.ijpharm.2016.04.023

Brozek-Pluska B, Orlikowski M, Abramczyk H (2016) Phthalocyanines: from dyes to photosensitizers in diagnostics and treatment of cancer—spectroscopy and raman imaging studies of phthalocyanines in human breast tissues. In: Kadish KM, Smith KM, Guilard R (eds) Handbook of porphyrin science, with applications to chemistry, physics, materials science, engineering, biology and medicine. World Scientific, UK/Singapore, pp 1–49

Carrera ET, Dias HB, Corbi SCT, Marcantonio RAC, Bernardi ACA, Bagnato VS, Hamblin MR, Rastelli ANS (2016) The application of antimicrobial photodynamic therapy (aPDT) in dentistry: a critical review. Laser Phys 26:123001. https://doi.org/10.1088/1054-660x/26/12/123001

Cheng G, Hao H, Xie S, Wang X, Dai M, Huang L, Yuan Z (2014) Antibiotic alternatives: the substitution of antibiotics in animal husbandry? Front Microbiol 5:217. https://doi.org/10.3389/fmicb.2014.00217

Chernii V, Tomachynski L, Gerasymchuk Y, St Radzki, Volkov S (2003) Synthesis and spectral properties of mixed-ligand zirconium and hafnium phthalocyanines with axially coordinated phthalic acids. Ukrainian Chem J 69(3):9–11

Cieplik F, Deng D, Crielaard W, Buchalla W, Hellwig E, Al-Ahmad A, Maisch T (2018) Antimicrobial photodynamic therapy: what we know and what we don't. Critic Rev Microbiol 44(5):571–589. https://doi.org/10.1080/1040841X.2018.1467876

Dougherty TJ (2002) An update on photodynamic therapy applications. J Clin Laser Med Surg 20(1):3–7. https://doi.org/10.1089/104454702753474931

Frieri M, Kumar K, Boutin A (2017) Antibiotic resistance. J Infect Pub Health 10(4):369–378. https://doi.org/10.1016/j.jiph.2016.08.007

Gacki M, Kafarska K, Pietrzak A, Korona-Głowniak I, Wolf WM (2020) Quasi-isostructural Co(II) and Ni(II) complexes with mefenamato ligand: synthesis, characterization, and biological activity. Molecules 25(13):3099. https://doi.org/10.3390/molecules25133099

Gao Y, Mai B, Wang A, Li M, Wang X, Zhang K, Liu Q, Wei Sh, Wang P (2018) Antimicrobial properties of a new type of photosensitizer derived from phthalocyanine against planktonic and biofilm forms of Staphylococcus aureus. Photodiagnosis Photodyn Therapy 21:316–326. https://doi.org/10.1016/j.pdpdt.2018.01.003

Gerasymchuk YS, Chernii VY, Tomachynskii LA, Kowalska M, Legendziewicz J, St Radzki (2010) Correlation between computer models of structure of 5-sulfosalicylato Zr(IV) phthalocyanine with results obtained by NMR, ESI-MS and UV–Vis spectra. Opt Mater 32:1193–1201

Gerasymchuk Y, Volkov S, Chernii V, Tomachynski L, St R (2004) Synthesis and spectral properties of axially substituted zirconium(IV) and hafnium(IV) water soluble phthalocyanines in solutions. J Alloys Compd 380:186–190. https://doi.org/10.1016/j.jallcom.2004.03.090

Gerasymchuk Y, Lukowiak A, Wedzynska A, Kedziora A, Bugla-Ploskonska G, Piatek D, Bachanek T, Chernii V, Tomachynski L, Strek W (2016) New photosensitive nanometric graphite oxide composites as antimicrobial material with prolonged action. J Inorg Biochem 159:142–148. https://doi.org/10.1016/j.jinorgbio.2016.02.019

Gerasymchuk Y, Łukowiak A, Kędziora A, Wędzyńska A, Bugla-Płoskońska G, Piątek D, Bachanek T, Chernii V, Tomachynski L, Stręk W (2017) New antibacterial photoactive nanocomposite additives for endodontic cements and fillings. In: Di Bartolo B, Collins J, Silvestri L (eds) Nano-optics: principles enabling basic research and applications—NATO science for peace and security series b: physics and biophysics. Springer, Dordrecht, pp 507–509

Gerasymchuk Y, Kałas W, Arkowski J, Marciniak Ł, Hreniak D, Wysokińska E, Strządała L, Obremska M, Tomachynski L, Chernii V, Stręk W (2021) Gallato zirconium (IV) phtalocyanine complex conjugated with $SiO_2$ nanocarrier as a photoactive drug for photodynamic therapy of atheromatic plaque. Molecules 26(2):260. https://doi.org/10.3390/molecules26020260

Gershkovich AA, Kibiriev VK (1992) Chemical synthesis of peptides. Naukova Dumka, Kiev

Ghosh C, Sarkar P, Issa R, Haldar J (2019) Alternatives to conventional antibiotics in the era of antimicrobial resistance. Trends Microbiol 27(4):323–338. https://doi.org/10.1016/j.tim.2018.12.010

Goldman MP (2007) Photodynamic therapy. Elsevier Ltd., Oxford

Kędziora A, Gerasymchuk Y, Sroka E, Bugla-Płoskońska G, Doroszkiewicz W, Rybak Z, Hreniak D, Stręk W (2013) Use of the materials based on partially reduced graphene-oxide with silver nanoparticle as bacteriostatic and bactericidal agent. Polim Med 43:129–134

Kędziora A, Wernecki M, Korzekwa K, Speruda M, Gerasymchuk Y, Łukowiak A, Bugla-Płoskońska G (2020) Consequences of long-term bacteria's exposure to silver nanoformulations with different physicochemical properties. Int J Nanomed 15:199–213. https://doi.org/10.2147/IJN.S208838

Kikuchi T, Mogi M, Okabe I, Okada K, Goto H, Sasaki Y, Fujimura T, Fukuda M, Mitani A (2015) Adjunctive application of antimicrobial photodynamic therapy in nonsurgical periodontal treatment: a review of literature. Int J Mol Sci 16:24111–24126. https://doi.org/10.3390/ijms161024111

Liu S, Wei L, Hao L, Fang N, Chang MW, Xu R, Yang Y, Chen Y (2009) Sharper and faster "nano darts" kill more bacteria: a study of antibacterial activity of individually dispersed pristine single-walled carbon nanotube. ACS Nano 3(12):3891–3902. https://doi.org/10.1021/nn901252r

Liu S, Zeng TH, Hofmann M, Burcombe E, Wei J, Jiang R, Kong J, Chen Y (2011) Antibacterial activity of graphite, graphite oxide, graphene oxide, and reduced graphene oxide: membrane and oxidative stress. ACS Nano 5(9):6971–6980. https://doi.org/10.1021/nn202451x

Lukowiak A, Gerasymchuk Y, Wedzynska A, Tahershamsi L, Tomala R, Strek W, Piatek D, Korona-Glowniak I, Speruda M, Kedziora A, Bugla-Ploskonska G (2019) Light-activated zirconium(IV) phthalocyanine derivatives linked to graphite oxide flakes and discussion on their antibacterial activity. Appl Sci 9(20):4447. https://doi.org/10.3390/app9204447

Mantareva VN, Angelov I, Wöhrle D, Borisova E, Kussovski V (2013) Metallophthalocyanines for antimicrobial photodynamic therapy: an overview of our experience. J Porphyr Phthalocyanines 17(06–07):399–416. https://doi.org/10.1142/S1088424613300024

Nathan C (2020) Resisting antimicrobial resistance. Nat Rev Microbiol 18:259–260. https://doi.org/10.1038/s41579-020-0348-5

Nwahara N, Nkhahle R, Ngoy BP, Mack J, Nyokong T (2018) Synthesis and photophysical properties of BODIPY-decorated graphene quantum dot–phthalocyanine conjugates. New J Chem 42:6051–6061. https://doi.org/10.1039/C8NJ00758F

Nyamu SN, Ombaka L, Masika E, Ng'ang'a M, (2018) Antimicrobial photodynamic activity of phthalocyanine derivatives Hindawi. Adv Chem 2018:2598062. https://doi.org/10.1155/2018/2598062

Nyokong T, Antunes E (2013) Influence of nanoparticle materials on the photophysical behavior of phthalocyanines. Coord Chem Rev 257:2401–2418. https://doi.org/10.1016/j.ccr.2013.03.016

Rajtar B, Skalicka-Woźniak K, Świątek Ł, Stec A, Boguszewska A, Polz-Dacewicz M (2017) Antiviral effect of compounds derived from Angelica archangelica L. on Herpes simplex virus-1 and Coxsackievirus B3 infections. Food Chem Toxicol 109:1026–1031. https://doi.org/10.1016/j.fct.2017.05.011

Saladino ML, Markowska M, Carmone C, Cancemi P, Alduna R, Presentato A, Scaffaro R, Biały D, Hasiak M, Hreniak D, Wawrzyńska M (2020) Graphene oxide carboxymethylcellulose nanocomposite for dressing materials. Materials 13:8. https://doi.org/10.3390/ma13081980

Sundqvist G, Figdor D, Persson S, Sjögren U (1998) Microbiologic analysis of teeth with failed endodontic treatment and the outcome of conservative re-treatment. Oral Surg Oral Med Oral Pathol Oral Radiol Endod 85(1):86–93. https://doi.org/10.1016/s1079-2104(98)90404-8

Szabó T, Tombácz E, Illés E, Dékány I (2006) Enhanced acidity and pH-dependent surface charge characterization of successively oxidized graphite oxides. Carbon 44:537–545. https://doi.org/10.1016/j.carbon.2005.08.005

Tahershamsi L, Gerasymchuk Y, Wedzynska A, Ptak M, Tretyakova I, Lukowiak A (2020) Synthesis, spectroscopic characterization and photoactivity of Zr(IV) phthalocyanines functionalized with aminobenzoic acid and their GO-based composites. J Carbon Res C 6:1. https://doi.org/10.3390/c6010001

Thema FT, Moloto MJ, Dikio ED, Nyangiwe NN, Kotsedi L, Maaza M, Khenfouch M (2013) Synthesis and characterization of graphene thin films by chemical reduction of exfoliated and intercalated graphite oxide. J Chem. https://doi.org/10.1155/2013/150536

Tomachinski LA, Chernii VY, Gorbenko KHN, Filonenko VV, Volkov SV (2003) Cytostatic antitumour activity of new mixed ligand zirconium phthalocyanine with lysine. Ukrainian Chem J 69(3):11–13

Tomachynski L, Chernii V, Gorbenko H, Volkov S (2001) Synthesis and properties of axially substituted zirconium (IV) and hafnium (IV) phthalocyanines with organic ligands. J Porphyr Phthalocyanines 5:731–734. https://doi.org/10.1002/jpp.384

Tomachynski LA, Chernii VY, Gorbenko HN, Filonenko VV, Volkov SV (2004) Synthesis, spectral properties, and antitumor activity of a new axially substituted phthalocyanine complex of zirconium(IV) with citric acid. Chem Biodivers 1(6):862–867. https://doi.org/10.1002/cbdv.200490068

Tomachynski L, Tretyakova I, Chernii V, Volkov S, Kowalska M, Legendziewicz J, Gerasymchuk Y, St Radzki (2008) Synthesis and spectral properties of Zr(IV) and Hf(IV)phthalocyanines with b-diketonates as axial ligands. Inor Chim Acta 361:2569–2581. https://doi.org/10.1002/jpp.384

Tretyakova IN, Chernii VY, Tomachynski LA, Volkov SV (2007) Synthesis and luminescent properties of new zirconium (IV) and hafnium (IV) phthalocyanines with various carbonic acids as outplaned ligands. Dyes Pigm 75:67–72. https://doi.org/10.1016/j.dyepig.2006.05.013

Wainwright M (1998) Photodynamic antimicrobial chemotherapy (PACT). J Antimicrob Chemother 42(1):13–28. https://doi.org/10.1093/jac/42.1.13

Zaman SB, Hussain MA, Nye R, Mehta V, Mamun KT, Hossain N (2017) A review on antibiotic resistance: alarm bells are ringing. Cureus 9(6):e1403. https://doi.org/10.7759/cureus.1403